nature cities

Supplementary information https://doi.org/10.1038/s44284-025-00240-y

Land subsidence risk to infrastructure in US metropolises

In the format provided by the authors and unedited

Table of Contents

Fig. 1. The Influence of Groundwater Extraction on Urban Subsidence in US Cities.

Fig. 2. Copula-based Simulation of Groundwater-Induced Vertical Land Motion (VLM) in New York, NY.

Fig. 3. Copula-based Simulation of Groundwater-Induced Vertical Land Motion (VLM) in Washington, D.C.

Fig. 4. Copula-based Simulation of Groundwater-Induced Vertical Land Motion (VLM) in Houston, TX.

Fig. 5. Copula-based Simulation of Groundwater-Induced Vertical Land Motion (VLM) in Memphis, TN.

Fig. 6. Copula-based Simulation of Groundwater-Induced Vertical Land Motion (VLM) in San Diego, CA.

Fig. 7. Standard Deviation Values of Vertical Land Motion (VLM) for 12 Most Populated US Cities.

Fig. 8. Standard deviation Values of Vertical Land Motion (VLM) across 12 US Cities.

Fig. 9. Standard deviation Values of Vertical Land Motion (VLM) across 4 US Cities.

Fig. 10. Validating the Vertical Land Motion (VLM) rates in US cities.

Fig. 11. Risk Matrix used to Estimate the Different Risk Categories.

Table 1. Documented Cases of Land Subsidence Across U.S. Cities in Scientific Literature.

Table 2. Population and vertical land motion (VLM) rates for US cities.

Table 3. Exposure to Urban Land Subsidence in US Cities.

Table 4. Hazard and Risks of Urban Land Subsidence in US Cities.

Table 5. Synthetic Aperture Radar (SAR) Datasets for US Cities.

Table 6. Information for Estimated Groundwater Withdrawal Datasets Analyzed in this Study.

Table 7. Information for Groundwater Well Datasets Analyzed in this Study.

Table 8. Goodness-of-fit criteria for Copula functions evaluated in this study.

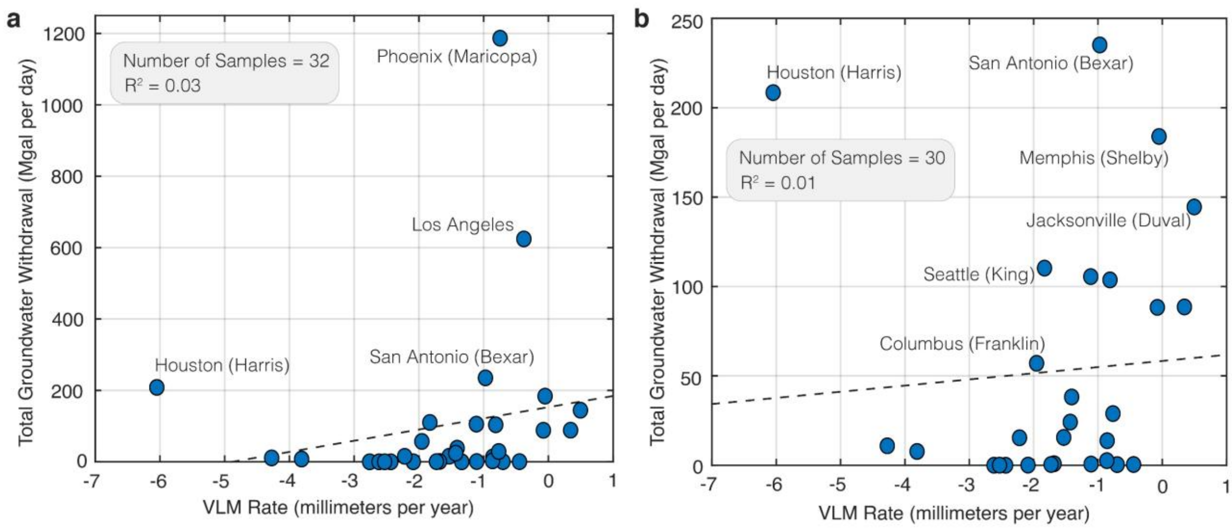

Fig. 1. The Influence of Groundwater Extraction on Urban Subsidence in US Cities. (a) Bivariate plot comparing vertical land motion (VLM) in mm per year versus total groundwater withdrawal in Mgal per day for all cities. **(b)** Bivariate plot comparing vertical land motion (VLM) in mm per year versus total groundwater withdrawal in Mgal per day for all cities excluding 2 cities (Phoenix and Los Angeles) with extreme groundwater withdrawal rates (>600 Mgal per day). The groundwater withdrawal data was obtained from Lovelace et al.[74] and Dieter et al.[75].

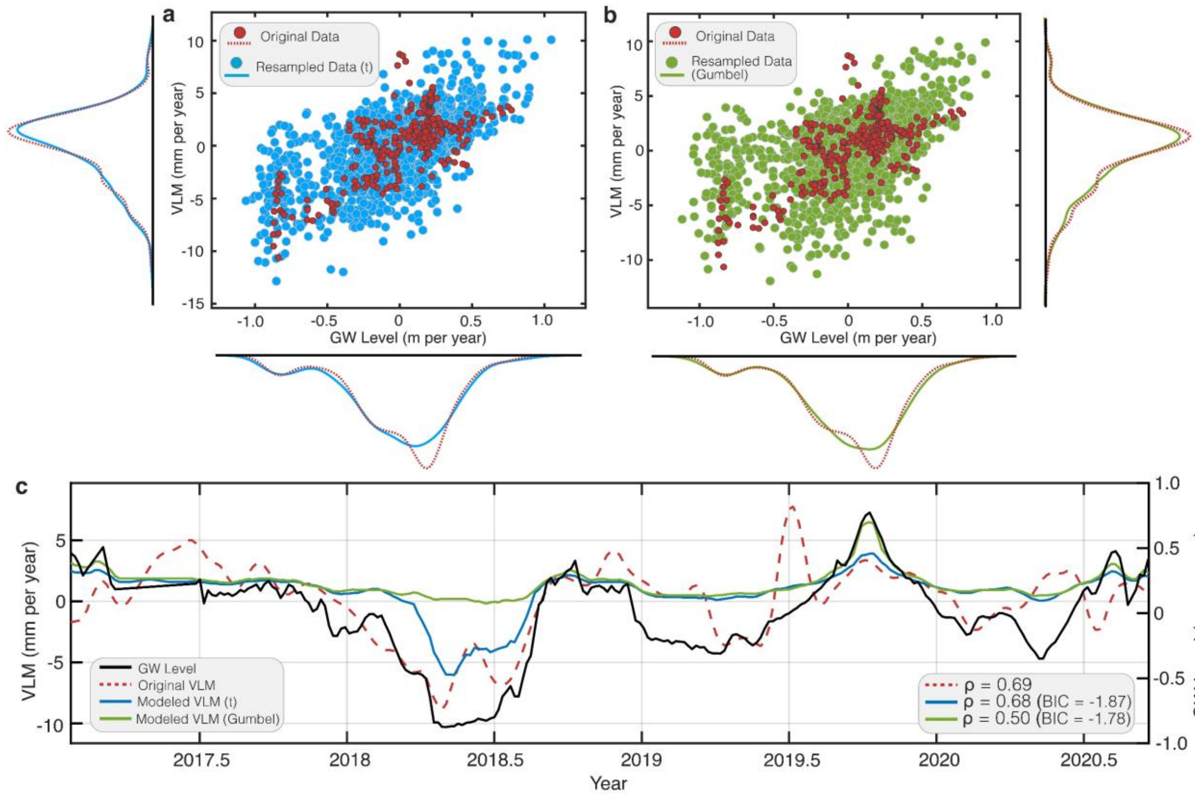

Fig. 2. Copula-based Simulation of Groundwater-Induced Vertical Land Motion (VLM) in New York, NY. (a, b) Scatter plots comparing empirical groundwater (GW) level trends and VLM (red points) with copula-resampled data from the **(a)** best-fitting model (t copula, blue) and **(b)** worst-fitting model (Gumbel copula, green). Marginal kernel density plots (bottom, left, and right axes) illustrate differences between observed and simulated distributions. **(c)** Detrended time series of observed GW levels (black) and VLM (red dashed) overlaid with copula-simulated VLM from the best- (blue solid line) and worst-fitting (green solid line) models. Correlation coefficients (ρ) and Bayesian Information Criterion (BIC) values quantify model performance.

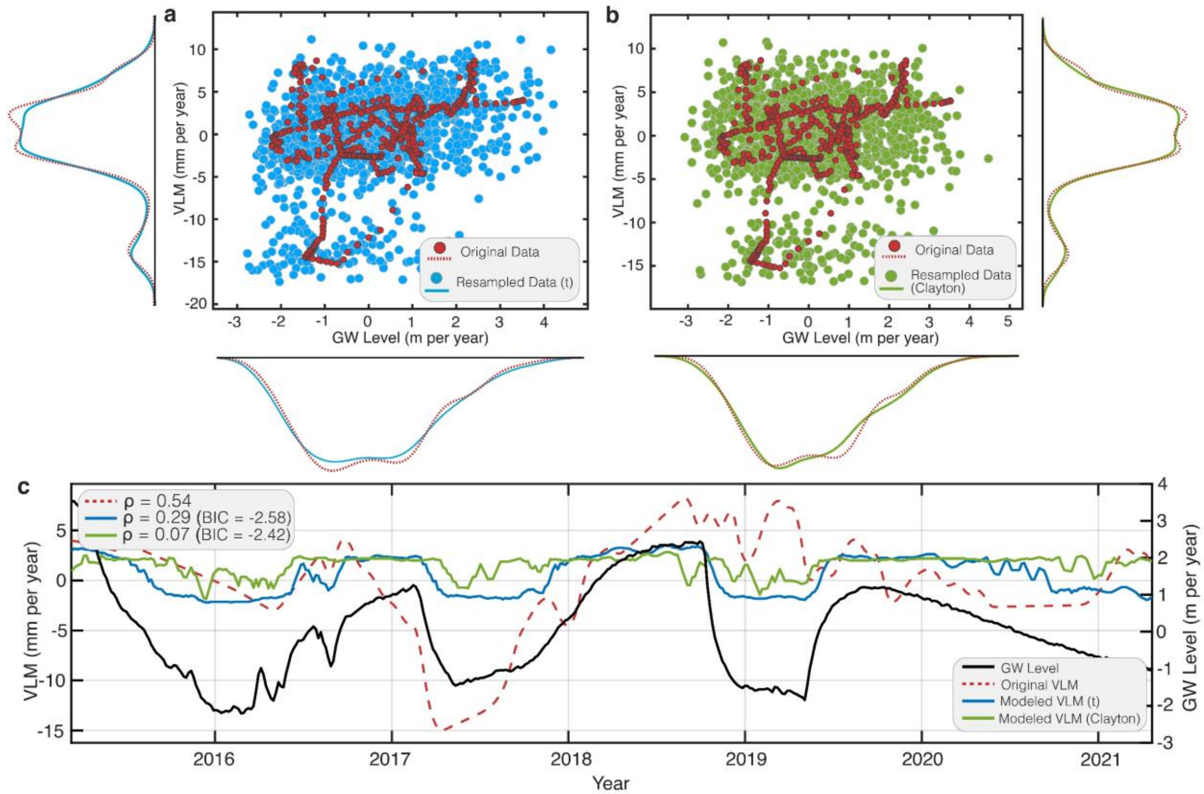

Fig. 3. Copula-based Simulation of Groundwater-Induced Vertical Land Motion (VLM) in Washington, D.C. (a, b) Scatter plots comparing empirical groundwater (GW) level trends and VLM (red points) with copula-resampled data from the **(a)** best-fitting model (t copula, blue) and **(b)** worst-fitting model (Clayton copula, green). Marginal kernel density plots (bottom, left, and right axes) illustrate differences between observed and simulated distributions. **(c)** Detrended time series of observed GW levels (black) and VLM (red dashed) overlaid with copula-simulated VLM from the best- (blue solid line) and worst-fitting (green solid line) models. Correlation coefficients (ρ) and Bayesian Information Criterion (BIC) values quantify model performance.

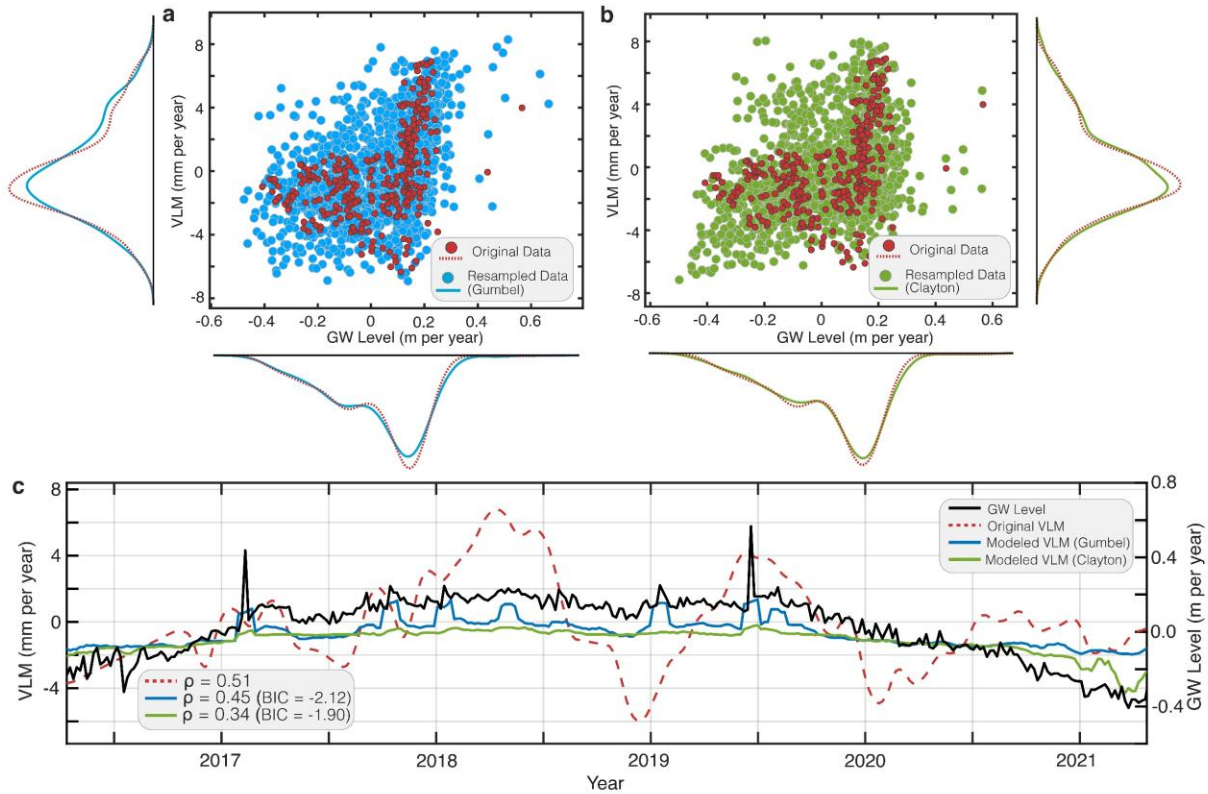

Fig. 4. Copula-based Simulation of Groundwater-Induced Vertical Land Motion (VLM) in Houston, TX. (a, b) Scatter plots comparing empirical groundwater (GW) level trends and VLM (red points) with copula-resampled data from the **(a)** best-fitting model (Gumbel copula, blue) and **(b)** worst-fitting model (Clayton copula, green). Marginal kernel density plots (bottom, left, and right axes) illustrate differences between observed and simulated distributions. **(c)** Detrended time series of observed GW levels (black) and VLM (red dashed) overlaid with copula-simulated VLM from the best- (blue solid line) and worst-fitting (green solid line) models. Correlation coefficients (ρ) and Bayesian Information Criterion (BIC) values quantify model performance.

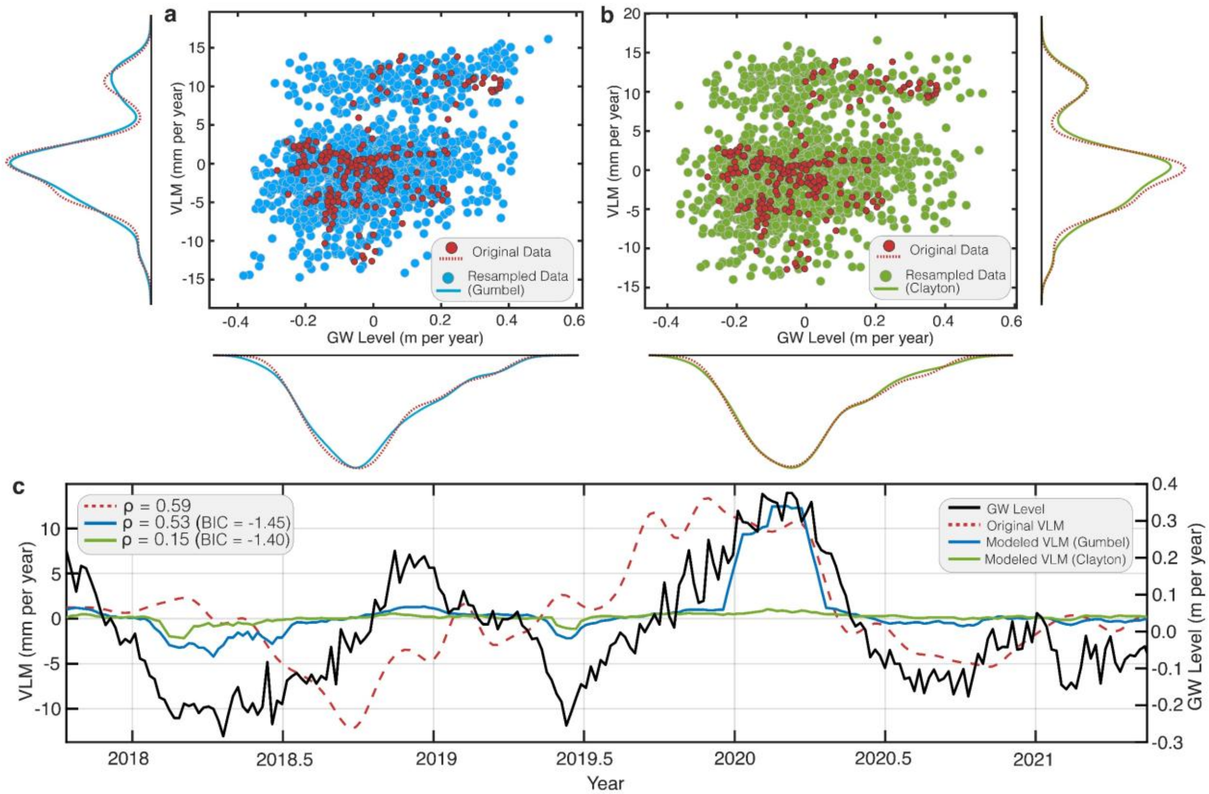

Fig. 5. Copula-based Simulation of Groundwater-Induced Vertical Land Motion (VLM) in Memphis, TN. (a, b) Scatter plots comparing empirical groundwater (GW) level trends and VLM (red points) with copula-resampled data from the **(a)** best-fitting model (Gumbel copula, blue) and **(b)** worst-fitting model (Clayton copula, green). Marginal kernel density plots (bottom, left, and right axes) illustrate differences between observed and simulated distributions. **(c)** Detrended time series of observed GW levels (black) and VLM (red dashed) overlaid with copula-simulated VLM from the best- (blue solid line) and worst-fitting (green solid line) models. Correlation coefficients (ρ) and Bayesian Information Criterion (BIC) values quantify model performance.

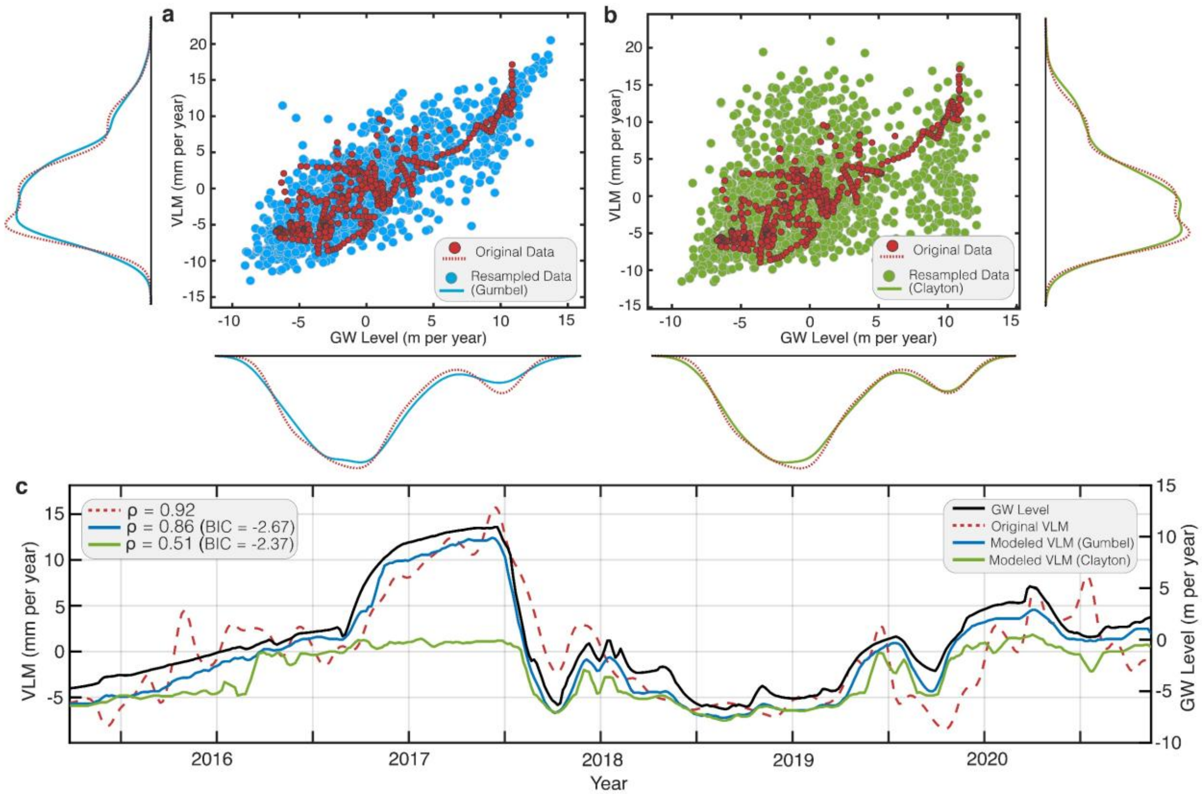

Fig. 6. Copula-based Simulation of Groundwater-Induced Vertical Land Motion (VLM) in San Diego, CA. (a, b) Scatter plots comparing empirical groundwater (GW) level trends and VLM (red points) with copula-resampled data from the **(a)** best-fitting model (Gumbel copula, blue) and **(b)** worst-fitting model (Clayton copula, green). Marginal kernel density plots (bottom, left, and right axes) illustrate differences between observed and simulated distributions. **(c)** Detrended time series of observed GW levels (black) and VLM (red dashed) overlaid with copula-simulated VLM from the best- (blue solid line) and worst-fitting (green solid line) models. Correlation coefficients (ρ) and Bayesian Information Criterion (BIC) values quantify model performance.

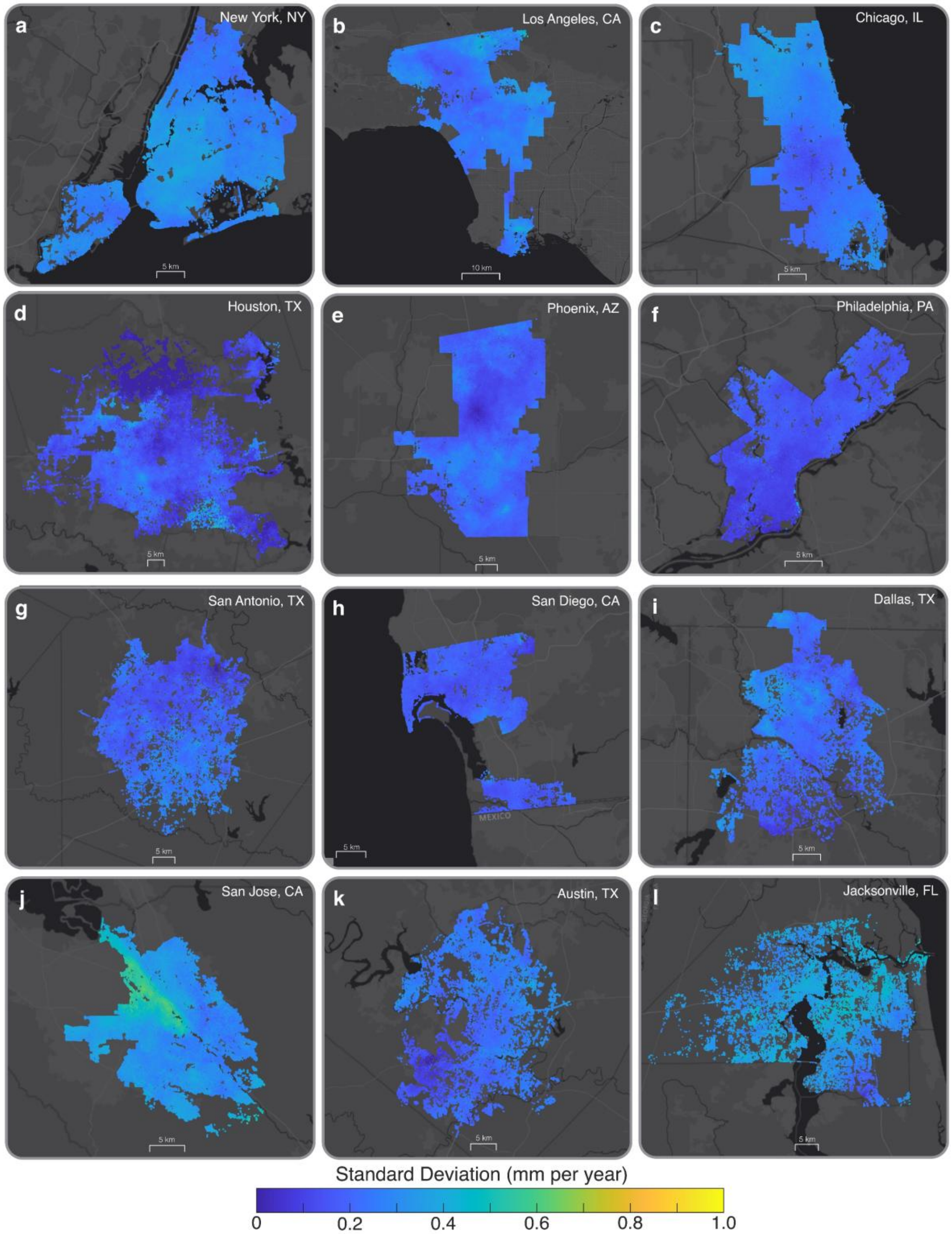

Fig. 7. Standard Deviation Values of Vertical Land Motion (VLM) for 12 Most Populated US Cities. Spatially varying standard deviation for **(a)** New York, NY, **(b)** Los Angeles, CA, **(c)** Chicago, IL, **(d)** Houston, TX, **(e)** Phoenix, AZ, **(f)** Philadelphia, PA, **(g)** San Antonio, TX, **(h)** San Diego, CA, **(i)** Dallas, TX, **(j)** San Jose, CA, **(k)** Austin, TX, **(l)** Jacksonville, FL. Background images: ESRI, streets-dark.

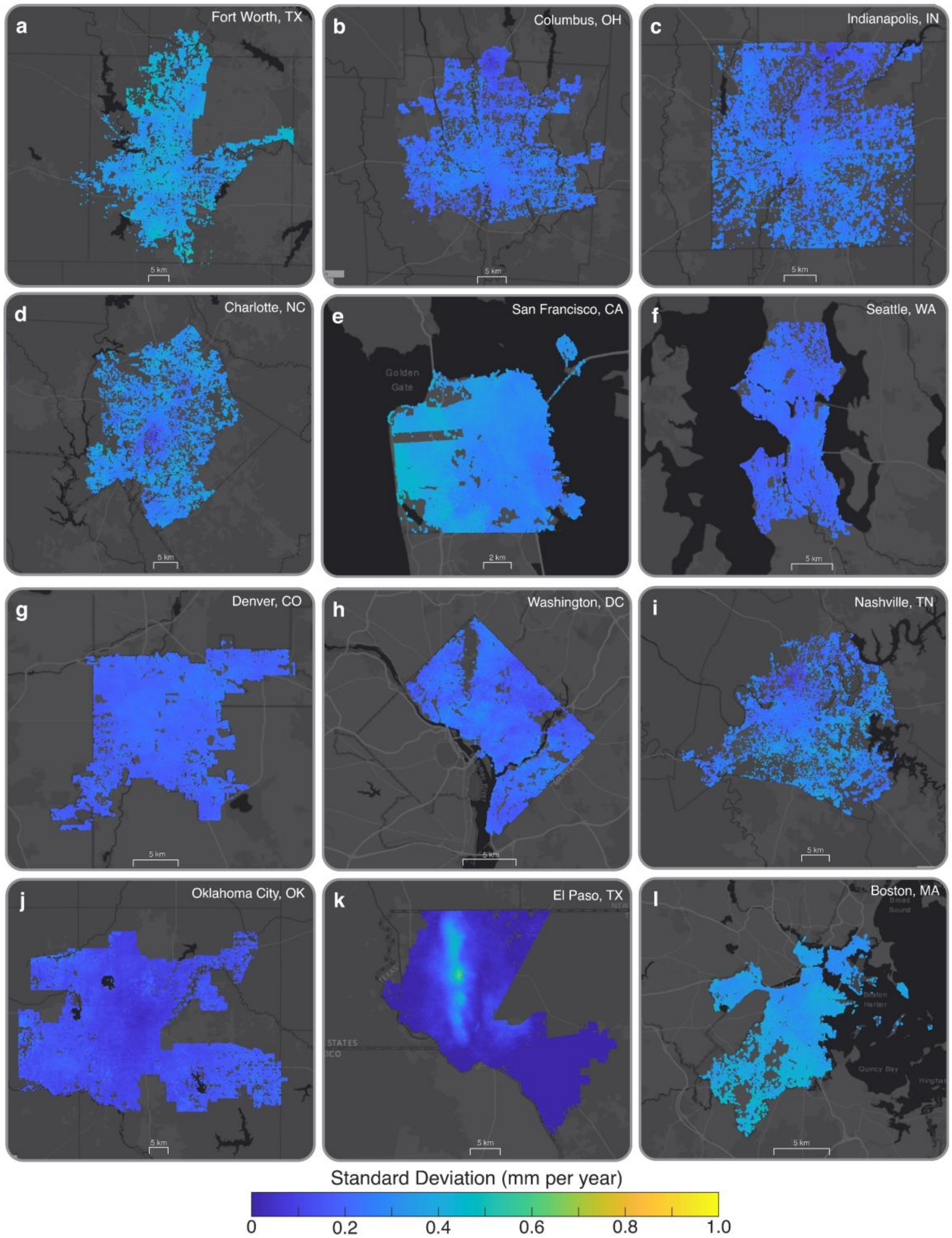

Fig. 8. Standard deviation Values of Vertical Land Motion (VLM) across 12 US Cities. Spatially varying standard deviation for **(a)** Fort Worth, TX, **(b)** Columbus, OH, **(c)** Indianapolis, IN, **(d)** Charlotte, NC, **(e)** San Francisco, CA, **(f)** Seattle, WA, **(g)** Denver, CO, **(h)** Washington, DC, **(i)** Nashville, TN, **(j)** Oklahoma City, OK, **(k)** El Paso, TX, **(l)** Boston, MA. Background images: ESRI, streets-dark.

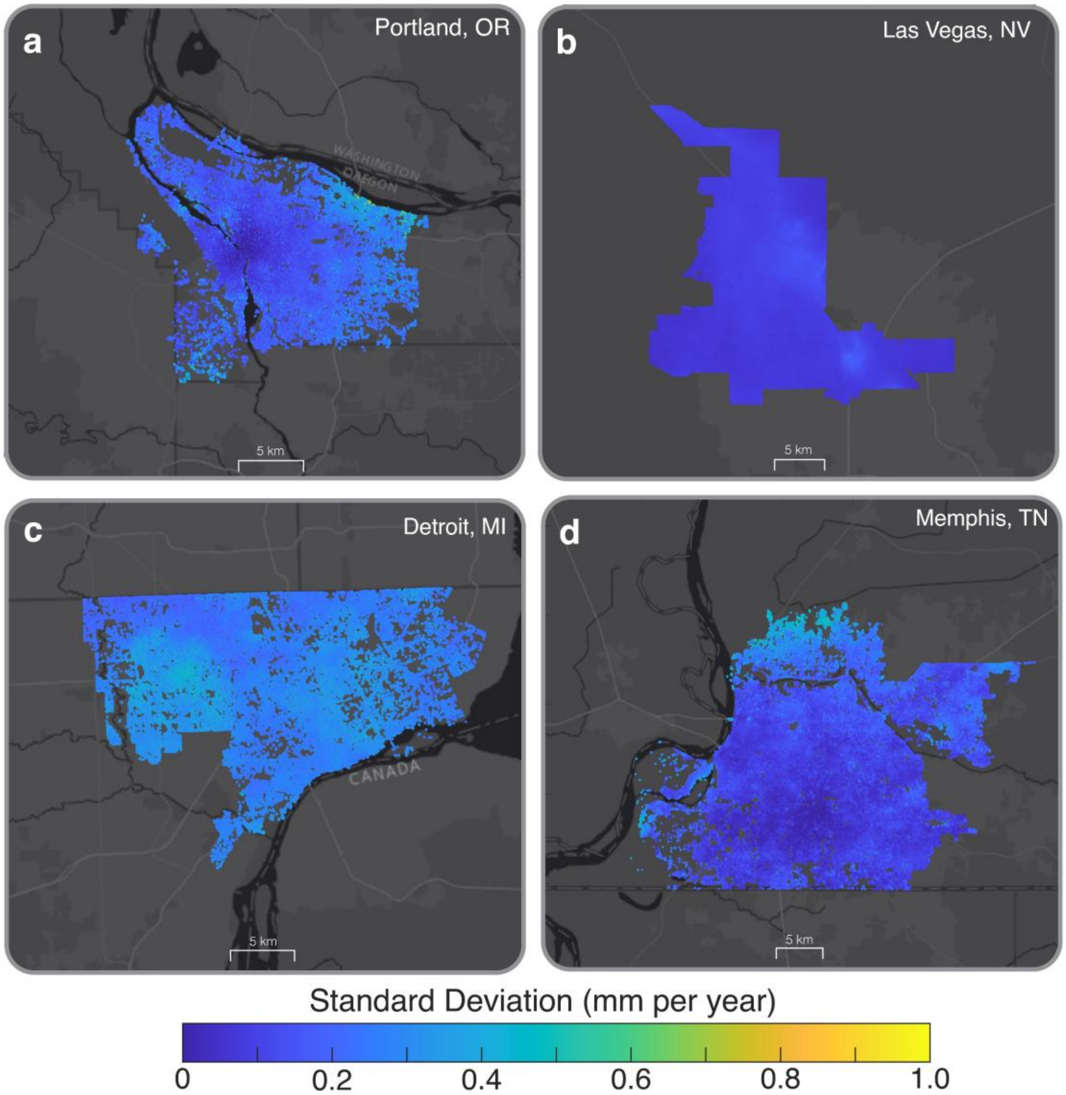

Fig. 9. Standard deviation Values of Vertical Land Motion (VLM) across 4 US Cities. Spatially varying standard deviation for **(a)** Portland, OR, **(b)** Las Vegas, NV, **(c)** Detroit, MI, **(d)** Memphis, TN. Background images: ESRI, streets-dark.

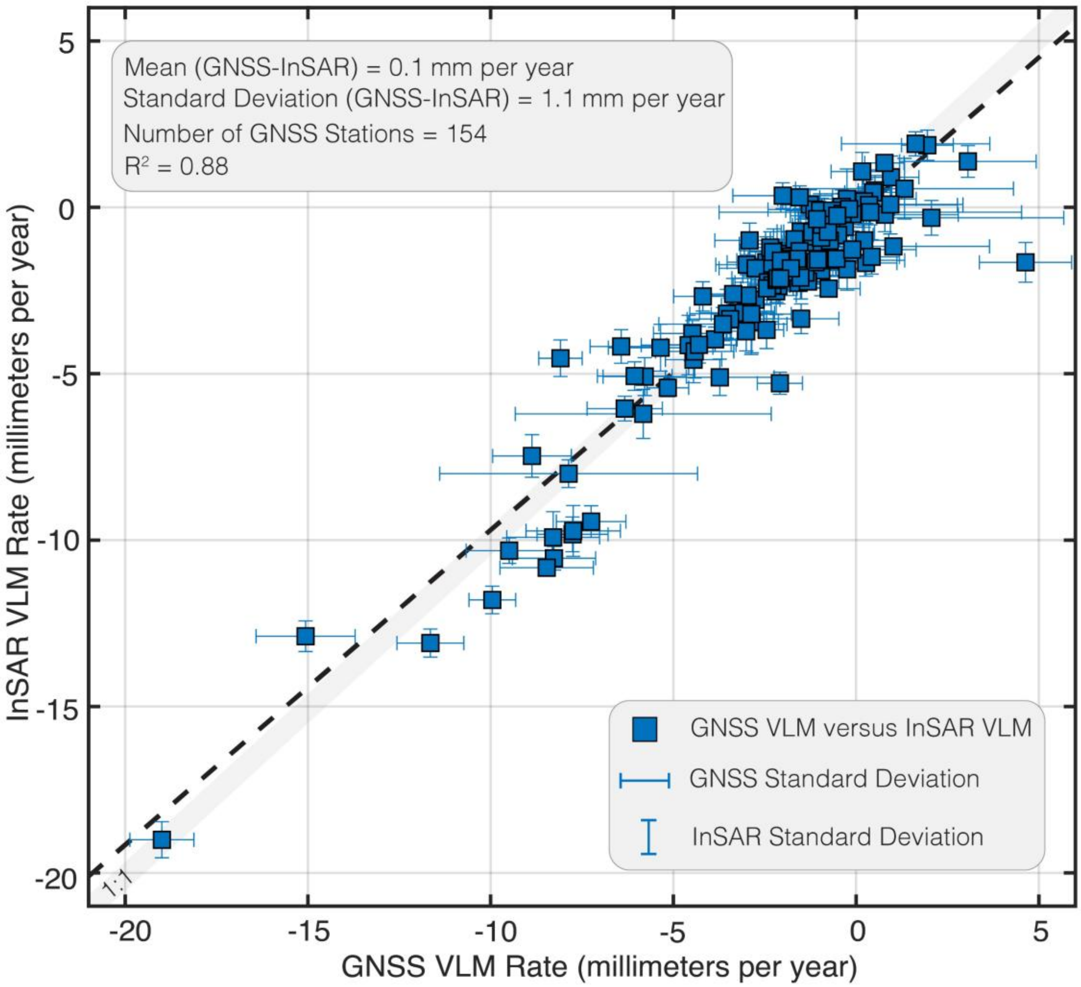

Fig. 10. Validating the Vertical Land Motion (VLM) rates in US cities. Bivariate plot comparing global navigation satellite system (GNSS) vertical rates with interferometric synthetic aperture radar (InSAR) derived VLM rates across the 28 US cities. The error bars show ±1 standard deviation for the GNSS and InSAR datasets. The comparison shows a R^2, mean difference, and standard deviation of 0.88, 0.1 mm per year, and 1.1 mm per year, respectively. The GNSS observations are obtained from the Nevada Geodetic Laboratory[64].

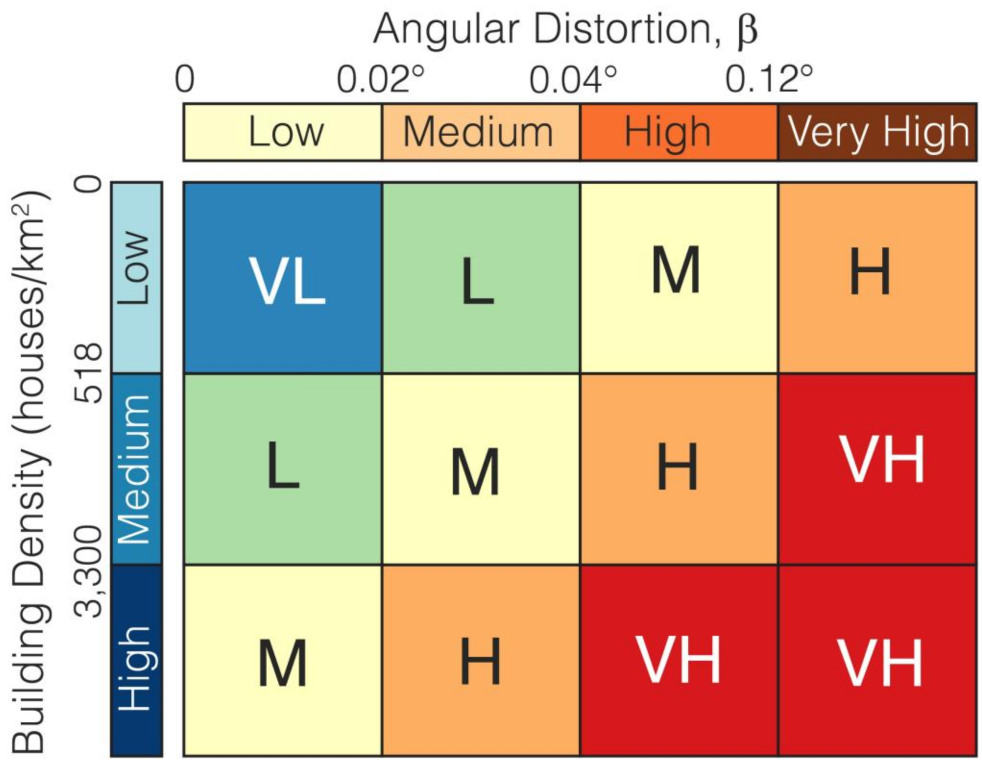

Fig. 11. Risk Matrix used to Estimate the Different Risk Categories. The risk matrix combines the severity of angular distortion hazard with the building exposure (i.e. building density) to estimate risk in 5 classes: Very Low – VL, Low – L, Medium – M, High – H, Very High – VH. The angular distortion hazard and risk maps for US cities are shown in Extended Data Figs. 3, 6, 7, 9, and 10.

Table 1. Documented Cases of Land Subsidence Across U.S. Cities in Scientific Literature. This table summarizes a systematic literature review of land subsidence across US cities. The literature review was conducted using Scopus, Web of Science and Google Scholar.

<See attached Excel sheet>

Table 2. Population and vertical land motion (VLM) rates for US cities. The population, average VLM, and area weighted VLM for the 28 US cities analyzed in this study. The population of each city is estimated from 2020 US Census data.

<See attached Excel sheet>

Table 3. Exposure to Urban Land Subsidence in US Cities. Area exposure is estimated in percentage (%) and population exposure is the number of people. The exposure is estimated for different levels of subsidence: not exposed to subsidence (VLM ≥ 0), 0 > VLM ≤ -3, -3 > VLM ≤ -5, -3 > VLM ≤ -10, VLM < -10. VLM values are in mm per year.

<See attached Excel sheet>

Table 4. Hazard and Risks of Urban Land Subsidence in US Cities. Area (km^2) affected by different angular distortion categories (low, medium, high, and very high) and the number of buildings for risk zones (VL: very low, L: low, M: medium, H: high, VH: very high).

<See attached Excel sheet>

Table 5. Synthetic Aperture Radar (SAR) Datasets for US Cities. The processed path and frame numbers for each city are indicated here. For ten cities, we processed multiple frames.

<See attached Excel sheet>

Table 6. Information for Estimated Groundwater Withdrawal Datasets Analyzed in this Study. The groundwater extraction data was obtained from https://www.sciencebase.gov/catalog/item/5d4a3c3ee4b01d82ce8dedc6.

<See attached Excel sheet>

Table 7. Information for Groundwater Well Datasets Analyzed in this Study. All groundwater well measurements were obtained from https://waterdata.usgs.gov/nwis/gw.

<See attached Excel sheet>

Table 8. Goodness-of-fit criteria for Copula functions evaluated in this study. The copula functions evaluated in this study are Gaussian, t, Clayton, Frank, and Gumbel.

<See attached Excel sheet>